Theor Chem Acc (2009) 123:93–103
DOI 10.1007/s00214-009-0547-7

REGULAR ARTICLE

Formation pathways of CH_3SOH from $CH_3S(OH)CH_3$ in the presence of O_2: a theoretical study

Juan M. Ramírez-Anguita · Àngels González-Lafont · José M. Lluch

Received: 13 February 2009 / Accepted: 13 February 2009 / Published online: 10 March 2009
© Springer-Verlag 2009

Abstract Methane sulfenic acid (CH_3SOH, MSEA) has been suggested in the literature as a possible stable product within the addition channel of the OH-initiated oxidation of dimethyl sulfide. In particular, it has been proposed as one of the thermodynamically feasible products of the reaction of $CH_3S(OH)CH_3$ adduct with O_2. However, MSEA has never been experimentally observed and a detailed theoretical analysis of all the reaction pathways leading to MSEA formation has never been reported. In this study, the first density functional and ab initio electronic structure calculations are carried out to characterize those reaction channels yielding MSEA. The adduct formed by the reaction of DMS-OH with O_2 ($CH_3S(O_2)(OH)CH_3$) has been taken as the starting point. On the other hand, a new reaction pathway, which competes with the MSEA formation yielding DMSO instead, is also presented. The kinetic relevance of those different reaction pathways is discussed to assert their contribution to the experimental measurements of the end-products of DMS-OH-initiated oxidation.

Keywords Methane sulfenic acid formation · OH-initiated oxidation of dimethyl sulfide · Gas-phase · Potential energy surface

Dedicated to Professor Santiago Olivella on the occasion of his 65th birthday and published as part of the Olivella Festschrift Issue.

Electronic supplementary material The online version of this article (doi:10.1007/s00214-009-0547-7) contains supplementary material, which is available to authorized users.

J. M. Ramírez-Anguita · À. González-Lafont (✉) · J. M. Lluch
Departament de Química, Universitat Autònoma de Barcelona, 08193 Bellaterra, Barcelona, Spain
e-mail: angels@klingon.uab.es

1 Introduction

Dimethyl sulfide (CH_3SCH_3, DMS) is known to be the main natural source of sulfur emissions released into the atmosphere. Both the natural and the anthropogenic sulfur-containing emissions take part in several environmental phenomena. During the daytime [1–5], sulfur-containing species are mainly oxidized by OH radicals, whereas NO_3 [6–8] radicals are the principal oxidant agents in night-time. In the absence of anthropogenic sources, the end-products of DMS oxidation in atmospheric conditions are known to become efficient cloud condensation nuclei (CCN) [9–11] and the main consequence of cloud formation is a regulatory effect in the amount of radiation which is able to pass the atmosphere in both ways.

The gas-phase OH-initiated oxidation of DMS has been extensively studied in the past. The experimental [1–4, 7, 12–19] and theoretical works [11, 20–26] already performed have contributed with a huge amount of information about the stable products obtained in those oxidation reactions. As a result, several DMS degradation mechanistic schemes have been built [7, 22, 26, 27]. It is well known by now that the distribution of DMS oxidation products has a close dependency on the temperature and the pressure conditions, and also on the presence of radical species, especially nitrogen oxides (NO_x) [5, 28, 29]. Those observations have led to the proposal of a two-channel OH-initiated oxidation process: the direct H-abstraction of DMS methyl-hydrogen atoms by the OH radical, and the reversible formation of $CH_3S(OH)CH_3$, DMS-OH adduct, which is scavenged by molecular oxygen. The H-abstraction channel is expected to yield SO_2, $CH_3SO_2OONO_2$ (MSPN), H_2SO_4, and CH_3SO_3H (MSA). On the other hand, the OH addition channel produces CH_3SOCH_3 (DMSO),

$CH_3SO_2CH_3$ ($DMSO_2$), and CH_3SO_2H (MSIA). It is not completely clear yet which is the real relevance in the atmosphere of each initiation channel, especially due to the complicated effect of environmental conditions on the distribution of oxidation end-products. In spite of this, relevant experimental kinetic information, in many cases obtained by measuring in the laboratory, the disappearance of the reactants (DMS and OH) has been published corresponding to several specific pathways of the proposed degradation mechanism. In addition, theoretical kinetic studies have also contributed to confirm several of those oxidation reactions that connect the initial reactants with several intermediates or stable products of the DMS degradation scheme.

The last published global scheme by Barnes et al. [7] for the OH and NO_3 radical-initiated oxidation of DMS is based on previous proposals by Yin et al. [11] and Ravishankara et al. [3, 4]. In their simplified scheme, Barnes et al. have marked the formation of methane sulfenic acid (CH_3SOH, MSEA) from the dissociation of the DMS-OH adduct, formed by the OH-addition to DMS, with dashed lines meaning that it is an uncertain channel. Within the OH-initiated global addition channel, the formation of MSEA could be a possible way to explain, at least partially, the product-yields dependence on the experimental conditions. In fact, Barnes et al. also indicate in their scheme that MSEA can in turn react with OH leading to the formation of CH_3SO, thus connecting the OH-initiated addition and H-abstraction parts of the global degradation scheme.

In fact, MSEA formation was already proposed by Ravishankara et al. [4] in 1996 as a thermodynamically feasible channel of the reaction between $CH_3S(OH)CH_3$ with O_2:

$$\text{DMS-OH} + O_2 \rightarrow CH_3OO + CH_3SOH \quad (1)$$

Very recently, Williams et al. [14] also included reaction (1) as a feasible channel for the reaction between the DMS-OH adduct with O_2 to form various potential products. Nevertheless, MSEA has never been experimentally detected as a stable product of the mentioned reaction. Furthermore, Gross et al. [22] rejected this proposal based on the following mechanism:

$$O_2 + CH_3S(OH)CH_3 \rightarrow [CH_3S(OH)CH_3 - OO]^* \quad (2)$$

$$[CH_3S(OH)CH_3 - OO]^* \rightarrow CH_3OO + CH_3S(OH) \quad (3)$$

that was not found to be a viable reaction pathway on the potential energy surface of that chemical mechanism at the PW91PW91/6-311G(d,p) level of electronic-structure theory. Gross et al. [3, 4, 11, 30] concluded that MSEA formation process does not occur under typical atmospheric conditions, also because the proposed mechanism could not agree with several experimental kinetic studies on the $OH + C(H/D)_3SC(H/D)_3$ reactions that did not reveal any kinetic isotope effect.

Note that in this mechanism a C···OO interaction is suggested in the intermediate complex instead of an S···OO bond, and the dissociation of that intermediate complex takes place by means of a sulfur carbon bond cleavage. The authors state that, in case MSEA was yielded, this would be the reaction sequence because the presence of an O_2 group stabilizes the S···OH bond, making the cleavage of the sulfur carbon bond more likely than for the DMS-OH molecule. In fact, the elimination reaction leading to MSEA and CH_3, via the dissociation of the DMS-OH adduct in the absence of O_2 by C···S bond cleavage, has already been included as a feasible process in previous studies [11]. Moreover, two of us analyzed in detail in a previous study [23] the reaction channels corresponding to the reaction between DMS + OH on the corresponding potential energy surface at several levels of electronic-structure theory. One of the main channels, denoted R1ac in that paper, was shown to proceed from reactants via a hydrogen-bonded complex in the entrance channel to the DMS-OH adduct which in the absence of molecular oxygen could then decompose following an elimination process with a saddle point structure located 12.22 kcal/mol above the bimolecular reactants in terms of adiabatic potential energy at the CCSD(T)/IB//MPW1K/MG3S level. The final dissociated products, CH_3SOH and CH_3, were calculated to be around 1.49 kcal/mol above the initial reactants in terms of classical potential energy. In a second paper by the same authors [25], the global kinetic constant for the DMS + OH reaction was calculated by means of Variational Transition State Theory. The elimination channel leading to MSEA and CH_3 was confirmed to be kinetically irrelevant in the global OH-initiated oxidation scheme of DMS due to the high energy barrier encountered for the dissociation of the DMS-OH adduct. The theoretical work performed up to now seems to be then in good agreement with the experimental data which do not indicate detection of MSEA in the DMS degradation process. Nevertheless, if MSEA reacts quickly, it is likely that it could not be detected. So then, under the suitable experimental conditions, it is possible that MSEA formation performs a relevant role in the whole mechanistic scheme.

In any case, no detailed theoretical analysis has ever been done to characterize the possible reaction pathways leading to MSEA as a final product. In this study, the first density functional and ab initio electronic structure calculations are carried out to characterize those reaction channels yielding MSEA. The adduct formed by the reaction of DMS-OH with O_2 ($CH_3S(O_2)(OH)CH_3$) has been taken as the starting point. On the other hand, a new reaction pathway which competes with the MSEA

formation yielding DMSO, instead, is also presented. These reaction pathways are analyzed and compared with each other and with other channels previously studied, with the main objective of inferring their kinetic relevance in the laboratory experiments that measure the product yields of the oxidation of the DMS in the presence of OH and O_2.

1.1 Computational methods

All the electronic structure calculations in this work were performed in the spin-restricted formalism for closed-shells and the spin-unrestricted formalism for open-shell systems.

Optimized geometries, energies, and first and second energy derivatives for the reactions were calculated by using hybrid density functional theory [31–34]. The selected hybrid functionals were the so-called MPW1K [35, 36] and M05-2X [37, 38]. The M05 density functional has also been used for one of the presented pathways. The fraction of Hartree–Fock (HF) exchange was optimized in MPW1K using a database of reaction energies and barrier heights, resulting in a value of 42.8%. This density functional has been tested against kinetic databases and it has shown a good compromise between cost and accuracy [36]. M05-2X and M05 [37] are hybrid meta-GGA functionals parameterized according to two criteria: the exchange functional is constrained to have the correct uniform electron gas (UEG) limit and its correlation functional is free of self-interaction. Several parameters were adjusted in both the exchange and the correlation functionals, as well as the percentage of HF exchange. The M05-2X HF exchange value is 56% [38]. It is accepted that HF exchange is an important parameter for describing the barrier heights of chemical reactions and the multireference character of a chemical system. In fact, no functional is expected to provide good results in barrier heights of chemical reactions unless the HF exchange is adequately high. In this sense, both MPW1K and M05-2X are fulfilling this constraint. On the other hand, the monodeterminantal reference used in the HF approximation is not suitable for describing multireference and transition-metal containing systems. So then, that parameter should be low when treating those kinds of systems. In accordance, the M05 density functional, with a 28% of HF exchange, has been proved [38] to be very accurate in describing systems with a large multireference character. However, this density functional gives also very good values for the barrier heights and the reaction energies of different kinds of chemical processes. For this reason, the M05 functional has very broad applicability in thermochemistry and kinetics.

In addition, two different sets of basis functions have been employed: the 6-31+G(d,p) basis set [39] from Pople's group and the MG3S basis set [40] from Truhlar's group. The systems which include sulfur atoms need of a large basis set to achieve accuracy in describing the electronic structure [41–43]. The MG3S basis set fulfills this requirement [40, 44].

The geometry optimizations and frequency calculations have been performed at the following levels: MPW1K/6-31+G(d,p), MPW1K/MG3S, and M05-2X/MG3S. The M05/6-31+G(d,p) and the M05/MG3S levels of calculation were used only in one reaction with a significant multireference character for achieving a better electronic description. The nature of the stationary points has been determined by means of the analysis of the number of imaginary frequencies: NIMAG = 1 for saddle points, or NIMAG = 0 for minima. The different channels were also characterized by means of constructing a minimum energy path [45, 46] (MEP, also known as IRC) between the stationary points found. The MEPs were performed at the MPW1K/6-31+G(d,p) level except for the reaction with a significant multireference character for which the M05/6-31+G(d,p) MEP was built. The calculation of those MEPs using the smaller basis set is justified because the 6-31+G(d,p) geometries are very similar to the ones obtained with the bigger MG3S basis set, even though the energetic description of the corresponding reaction pathways is much more basis-dependent. For this reason, only the MG3S energy results will be presented.

We have also carried out higher level single-point energy calculations with the aim of improving the electronic description of the chemical systems. Energies at all the stationary points were then recalculated at a higher level of theory, the CCSD(T) [47, 48]. Within this level of calculation, we have chosen the frozen core option. A recent study [49] has shown that this approximation gives similar energies to the ones obtained by choosing the full-electron correlated option within the coupled cluster approximation. In particular, the CCSD(T)/MG3S combination of the MG3S basis set with the CCSD(T) [49] energy is a good choice to balance the accuracy and computational cost for large systems. For the reaction with multireference character, the M05/MG3S energy values have been taken as the most accurate.

Quasi-thermodynamic magnitudes were computed by using the statistical thermodynamic formulation of partition functions within the ideal gas, rigid rotor, and harmonic oscillator models. The kinetic formulation, that is the standard state of 1 mol L^{-1}, has been adopted to give Gibbs free energy barriers in accordance with Transition State Theory (TST). The harmonic frequencies were corrected for anharmonicity with a scale factor 0.9581 at the MPW1K/MG3S level [50], 0.9642 at the M05-2X/MG3S level [51], and 0.9789 at the M05/MG3S level [51]. The quasi-thermodynamic magnitudes for the high-level electronic calculations we present (Gibbs free energy and adiabatic potential energy) were determined by using the

frequency calculations at the MPW1K/MG3S level, and at the M05/MG3S level for the reaction with multireference character, modified by the corresponding scale factors.

Gibbs free energies (G) are calculated for the stationary points at the CCSD(T)/MG3S//MPW1K/MG3S level of calculation and at the M05/MG3S level in one case. Classical potential energies (V) and adiabatic potential energies (V_a^G), that is including the zero point ground state energy corrections, at the MPW1K/MG3S, M05/MG3S, and the M05-2X/MG3S and CCSD(T)/MG3S//MPW1K/MG3S levels are also presented by means of Tables.

The optimizations, frequency calculations and single-point energy calculations were carried out with the Gaussian'03 [52] package program. The MEPs were performed with the Gaussian'03 package program by using the Gonzalez–Schlegel algorithm [53] and with the Gaussrate [54] package program following the Page–McIver algorithm [55, 56].

2 Results and discussion

To achieve our goal of finding any feasible pathways leading to MSEA formation, the following reactions have been considered in this study:

$$CH_3S(O_2)(OH)CH_3 \rightarrow CH_3SOH + CH_3 + O_2/CH_3SOH + CH_3O_2 \quad (R1)$$

$$CH_3S(O_2)(OH)CH_3 \rightarrow CH_3S(OH)CH_2(HO_2) \quad (R2)$$

$$CH_3S(OH)CH_2(HO_2) \rightarrow CH_3S(OH) + H_2O_2 + CH_2O \quad (R3)$$

$$CH_3S(OH)CH_2(HO_2) \rightarrow CH_3S(OH)CH_2OOH \rightarrow CH_3SOH + CH_2OOH/CH_3SOH + CH_3OO \quad (R4)$$

$$CH_3S(OH)CH_2(HO_2) \rightarrow CH_3SOCH_3 + HO_2. \quad (R5)$$

The most relevant novelty regarding previous suggestions of MSEA formation pathways is the starting point considered here, the $CH_3S(O_2)(OH)CH_3$ adduct. In this respect, we have taken into account a previous study [22] in which, although the O_2 reaction with DMS-OH was considered as the most likely MSEA formation pathway, it was concluded that MSEA was not yielded from the attack of O_2 to either carbon atom of DMS-OH forming a C···O_2 bond. Also in the Sect. 1, it has been mentioned that Barnes et al. [7] showed in their degradation scheme that the DMS-OH adduct should be the most likely MSEA precursor. Nevertheless, no specific mechanistic proposal was given in their review. In addition, as pointed out previously, the direct decomposition of DMS-OH into MSEA and CH_3 has been shown to be a clearly slower kinetic process in comparison with other competitive reactions [23]. All these previous considerations led us to propose that the $CH_3S(O_2)(OH)CH_3$ adduct, formed by the attack of the O_2 molecule to the sulfur atom of DMS-OH, could act as a feasible starting point. The reaction R1 is the direct decomposition of this adduct into MSEA and the CH_3O_2 radical, although CH_3 and O_2 has also been obtained as a final product. The reaction R2 leads to the formation of the $CH_3S(OH)CH_2(HO_2)$ radical, which is expected to be the common origin for the reactions R3, R4, and R5. Both the reactions R3 and R4 lead to MSEA formation from this radical. On the other hand, DMSO is also obtained from this chemical species, but according to the reaction R5. Classical potential energies, adiabatic potential energies at the MPW1K/MG3S, M05-2X/MG3S and CCSD(T)/MG3S//MPW1K/MG3S levels along with the Gibbs free energies at this last level are calculated at all the stationary points of R2, R3, R4, and R5. For the R1 reaction, results at the M05/MG3S level are given. From here on in the text, we will just refer to the energetic results at the CCSD(T)/MG3S//MPW1K/MG3S level, but for reaction R1 at the M05/MG3S level.

In the first place, it has to be mentioned that the $CH_3S(O_2)(OH)CH_3$ adduct presents four stable conformers [22], denominated C1, C2 C3, and C4, whose geometries differ in the relative orientation of the O_2 and the OH groups, both directly bonded to the sulfur atom. The geometries of those four complexes as well as the geometries for the corresponding saddle point structures that connect the four minima are shown in Figures S1 and S2 in the Supplementary Material. The classical and adiabatic potential energies along with the free energy profile for the stationary points of the exchange process of the different $CH_3S(O_2)(OH)CH_3$ conformations are also included in the Supplementary Material given with respect to DMS-OH and O_2 as reactants. It can be observed that, in agreement with Gross et al., complexes C3 and C4 are nearly degenerate and both lie around 3 kcal/mol below complexes C1 and C2 in terms of free energy. In what follows, a certain population of the four conformers was assumed in searching for possible MSEA pathways.

The stationary points for reaction R1, depicted in Fig. 1, have been characterized at the M05/MG3S level. This R1 pathway when initiated at the C3 conformer (R1a channel) leads to the adduct dissociation into three different products (MSEA, CH_3 and O_2) through the saddle point SP1a. At this saddle point structure, one methyl and the O_2 groups are loosing their corresponding interactions with the sulfur atom (S···CH_3 = 2.473 Å, S···O = 2.722 Å). According to the MEP performed for this pathway, the decomposition of the C3 adduct seems to take place in a

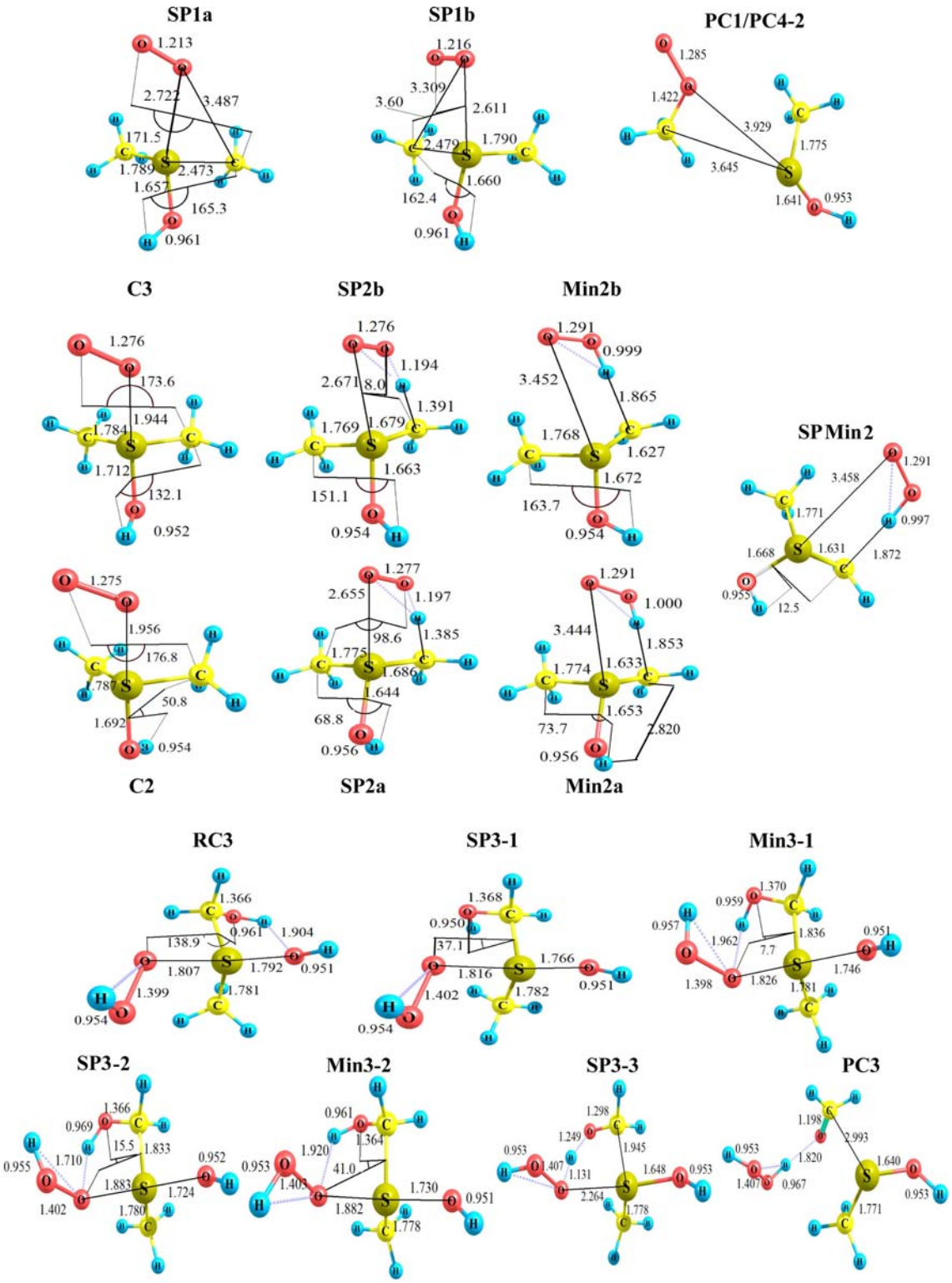

Fig. 1 Geometries of the stationary points located for the reactions R1 (M05/MG3S), R2 and R3 (MPW1K/MG3S). Distances are given in Å. Dihedrals are given in degrees

rather asynchronic way. The O_2 group does not begin to move away from the sulfur atom until the S···O distance is around 2.4–2.5 Å. At this point, the S···CH_3 distance starts to increase, while the O_2 group keeps on moving away from the sulfur atom. On the product side the MEP attains a flat region where the three dissociation fragments are

Table 1 Energies of the stationary points for the reaction R1 at different levels of calculation

	V_{C3}	$(V_a^G)_{C3}$	$V_{SP1a}^{\ddagger}$	$(V_a^G)_{SP1a}^{\ddagger}$	$V_{MSEA+CH_3+O_2}$	$(V_a^G)_{MSEA+CH_3+O_2}$
M05/MG3S	−14.4	−11.2	19.7	19.4	15.1	11.8
	V_{C4}	$(V_a^G)_{C4}$	$V_{SP1b}^{\ddagger}$	$(V_a^G)_{SP1b}^{\ddagger}$	V_{PC1}	$(V_a^G)_{PC1}$
M05/MG3S	−14.3	−10.9	19.4	19.3	−21.3	−18.4
	$V_{MSEA+CH_3O_2}$		$(V_a^G)_{MSEA+CH_3O_2}$			
M05/MG3S	−6.3		−3.1			
	$G_{MSEA+CH_3+O_2}$		$G_{MSEA+CH_3O_2}$			
M05/MG3S	3.8		−3.9			

V and V_a^G stand for the classical potential energies and the adiabatic potential energies, respectively. G stands for the Gibbs free energies of the feasible products. All energies (in kcal/mol) are relative to DMS-OH + O_2

already formed, but a minimum energy structure corresponding to a product complex could not be located. When initiated at the C4 conformer, the R1 pathway (channel R1b) leads via the saddle point SP1b to a product complex in which two dissociation products, MSEA and CH_3O_2, maintain a long-range interaction. The elimination of the CH_3O_2 radical is facilitated at the C4 adduct, because the oxygen atom of the O_2 group not bonded to the sulfur atom is already closer to one methyl carbon than at C3 (O···C distance is 2.948 Å at C3 and 2.889 Å at C4). The MEP of this R1b channel reveals also a rather asynchronic path: first, it is mainly the O_2 fragment that moves away from the sulfur atom, and afterwards begins the separation of CH_3. The difference with respect to the R1a channel is that the O_2 and CH_3 groups progressively approach each other as the MEP advances to the products side. As can be observed in the figures presented in Table 1, the two R1 channels are nearly energetically degenerated at the reactants and the saddle point regions, but are clearly different at the products region being channel R1b lower in energy. Channel R1a results in an endoergonic process by 3.8 kcal/mol with respect to DMS-OH + O_2, whereas channel R1b is exoergonic (−3.9 kcal/mol) at the M05/MG3S level. So MSEA and CH_3O_2 are the products thermodynamically favored. In any case, the high adiabatic potential energy barriers encountered along the two R1 channels (of around 19 kcal/mol) are so high that the kinetic relevance of those two MSEA formation channels is probably very low.

At this point, however, a comment on the suitability of the electronic-structure method used for this system must be given. In these R1 processes, a doublet molecule dissociates through saddle point regions where three fragments (a doublet radical, a triplet radical and a singlet molecule) interact, evolving to either the three separated products of R1a or the two (doublet + singlet) mentioned for the reaction R1b. Such complicated reactions are likely not to be well described with monoreferential methods. In effect, no saddle point could be located using the MPW1K density functional. In addition, the T1 diagnostic at the SP1a geometry calculated at the CCSD(T)/MG3S//M05/MG3S level turns out to be 0.16768, a huge value that reflects the large nondynamical effects present. This is the reason why the M05 density functional was used, because it has been shown to be very accurate in describing barrier heights and reaction energies of chemical processes as well as systems with a large multireference character. Given the difficulty of the problem, we are not confident of the accuracy of the M05 results, but at least we think that this method provides an estimation of the magnitude of the energy barriers. In this sense, as explained above, we think that the MSEA formation through the R1 channels can be discarded.

By means of reaction R2, the $CH_3S(OH)CH_2(HO_2)$ radical is formed. Two conformations of this radical have been located (Min2a/Min2b in Fig. 1), which are connected with the C2 and C3 conformers of the $CH_3S(O_2)(OH)CH_3$ adduct by means of the saddle points SP2a and SP2b, respectively (see Fig. 1). The OO···S interaction, which is present at the reactant adducts, gradually disappears while the O_2 group gets closer to one methyl-hydrogen at the saddle points SP2a and SP2b. The main distinction between those two saddle point geometries is the hydroxyl orientation with respect to the methyl groups. This structural difference is already present in C2 when compared with C3 as in the former structure the OH group is pointing to the opposite face of the methyl groups, whereas at C3 the hydroxyl and methyl groups are pointing to the same face. That geometrical difference is maintained along the two R2 paths until the product minima are located, being the CSOH dihedral angle value of 73.7° at Min2a and of 163.7° at Min2b. These two minima are also connected by means of a saddle point structure, denoted

Table 2 Energies of the stationary points for the reaction R2 at different levels of calculation

	V_{C2}	$(V_a^G)_{C2}$	$V^{\ddagger}_{SP2a}$	$(V_a^G)^{\ddagger}_{SP2a}$	V_{Min2a}	$(V_a^G)_{Min2a}$
MPW1K/MG3S	−10.0	−6.6	4.3	4.4	0.9	3.0
M05-2X/MG3S	−15.8	−13.9	0.5	0.0	−2.4	−0.1
CCSD(T)/MG3S//MPW1K/MG3S	−14.2	−10.7	1.1	1.1	−1.8	0.3
	V_{C3}	$(V_a^G)_{C3}$	$V^{\ddagger}_{SP2b}$	$(V_a^G)^{\ddagger}_{SP2b}$	V_{Min2b}	$(V_a^G)_{Min2b}$
MPW1K/MG3S	−13.1	−9.5	3.3	3.5	−0.2	2.1
M05-2X/MG3S	−18.8	−15.7	−0.4	−0.9	−3.5	−2.0
CCSD(T)/MG3S//MPW1K/MG3S	−17.3	−13.8	0.7	0.9	−3.1	−1.6

V and V_a^G stand for the classical potential energies and the adiabatic potential energies, respectively. All energies (in kcal/mol) are relative to DMS-OH + O_2

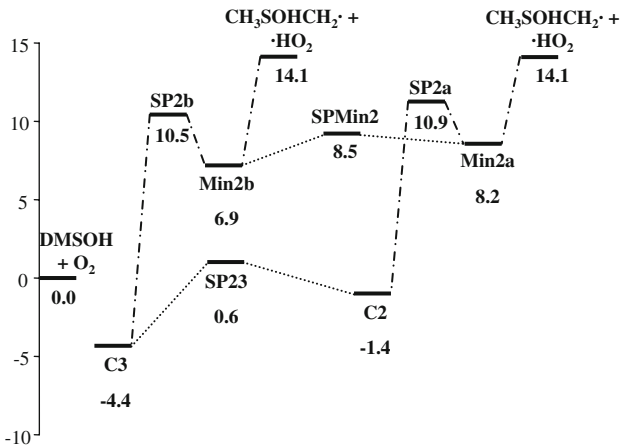

Fig. 2 CCSD(T)/MG3S/MPW1K/MG3S Gibbs free energy (kcal/mol) profile at 298 K for the reaction R2

SPMin2 in Fig. 1, which corresponds to the rotation of the OH group. The OO···H distance at the two saddle points SP2a and SP2b indicate the H abstraction is nearly completed. In Table 2, it can be observed that those two saddle points are nearly degenerate in terms of classical and adiabatic potential energies, whereas the R2b channel presents lower energies at the reactants and products regions. The free energy profiles presented in Fig. 2 show the same tendency although the inclusion of thermal and entropic contributions increases the H-abstraction barriers up to 10.9 and 10.5 kcal/mol with respect to DMS-OH + O_2 at SP2a and SP2b, respectively. On the other hand, tunneling effects could contribute to accelerate those two H-transfer processes. In addition, the stability of the different complexes is reduced in terms of free energy, resulting the formation of Min2a and Min2b as well as the formation of the final dissociated products from both channels clearly endoergonic.

Reactions R3, R4, and R5 initiate from the structures Min2a and/or Min2b of the R2 pathway. In first place, the reaction pathway R3, which is the reaction of $CH_3S(OH)CH_2(HO_2)$ with hydroxyl radical, is presented. The geometries of the stationary points are depicted in Fig. 1, and the classical potential energies along with the adiabatic potential energies are included in Table 3. According to our results, the hydroxyl group could attack this radical when the conformation Min2b is reached, thus leading to the formation of the RC3 structure in which a new $H_2C\cdots OH$ bond is formed while the OOH group has lost its H···C interaction and has formed a HOO···S bond, instead. The RC3 complex presents a huge stabilization free energy of 75.4 kcal/mol with respect to Min2b and OH that can be seen in Fig. 3, where the complete R3 free energy profile has been depicted. Also note that the incoming hydroxyl group is far from the HOOS group, but this situation changes when the saddle point SP3-1 is reached and especially at the minimum complex Min3-1, basically due to a variation in the dihedral angle HOO-S-CH_2-OH that changes from a value of 139.0° at RC3, to 37.2° at SP3-1, and finally to 7.8° at Min3-1. This intramolecular rotation around the S···C bond approaches the CH_2OH and HOOS groups. However, this reorganization still continues when the hydroxylic hydrogen belonging to the CH_2OH group is forced to approach the oxygen atom bonded to the sulfur atom in the SOOH fragment. A conformational change around the SO···OH bond changes the orientation of this OH group, which is pointing to the CH_2OH side of the molecule at Min3-1, but that is pointing to the other side at Min3-2. The SP3-2 structure connects Min3-1 and Min3-2. The analysis of the $CH_2O\underline{H}\cdots S\underline{O}OH$ distance (1.962 Å at Min3-1, 1.710 Å at SP3-2, 1.920 Å at Min3-2) shows the importance of the conformational change around the SO···OH bond. Note that the distance $CH_2O\underline{H}\cdots S\underline{O}OH$, which was expected to be the most similar parameter to the reaction coordinate, changes unexpectedly in the reaction path that connects Min3-1, SP3-2 and Min3-2. Once Min3-2 is reached, the SP3-3 and the PC3 stationary points are located basically by decreasing $CH_2O\underline{H}\cdots S\underline{O}OH$ distance. At SP3-3, the OOH

Table 3 Energies of the stationary points for the reaction R3 at different levels of calculation

	V_{RC3}	$(V_a^G)_{RC3}$	$V^{\ddagger}_{SP3-1}$	$(V_a^G)^{\ddagger}_{SP3-1}$	V_{Min3-1}	$(V_a^G)_{Min3-1}$	$V^{\ddagger}_{SP3-2}$	$(V_a^G)^{\ddagger}_{SP3-2}$
MPW1K/MG3S	−84.5	−77.3	−75.7	−69.1	−83.0	−75.6	−82.5	−75.7
M05-2X/MG3S	−95.2	−87.7	−86.3	−79.5	−93.6	−86.2	−92.9	−86.2
CCSD(T)/MG3S//MPW1K/MG3S	−92.5	−85.3	−83.9	−77.3	−91.1	−83.8	−90.7	−84.0

	V_{Min3-2}	$(V_a^G)_{Min3-2}$	$V^{\ddagger}_{SP3-3}$	$(V_a^G)^{\ddagger}_{SP3-3}$	V_{PC3}	$(V_a^G)_{PC3}$	$V_{MSEA+CH_2O+H_2O_2}$	$(V_a^G)_{MSEA+CH_2O+H_2O_2}$
MPW1K/MG3S	−85.3	−78.2	−75.5	−71.8	−88.2	−84.1	−78.0	−76.4
M05-2X/MG3S	−96.1	−88.8	−86.7	−82.6	−97.5	−92.6	−97.0	−96.4
CCSD(T)/MG3S//MPW1K/MG3S	−93.6	−86.6	−83.2	−79.4	−100.1	−96.0	−86.9	−85.5

V and V_a^G stand for the classical potential energies and the adiabatic potential energies, respectively. All energies (in kcal/mol) are relative to reactants (Min2b + OH)

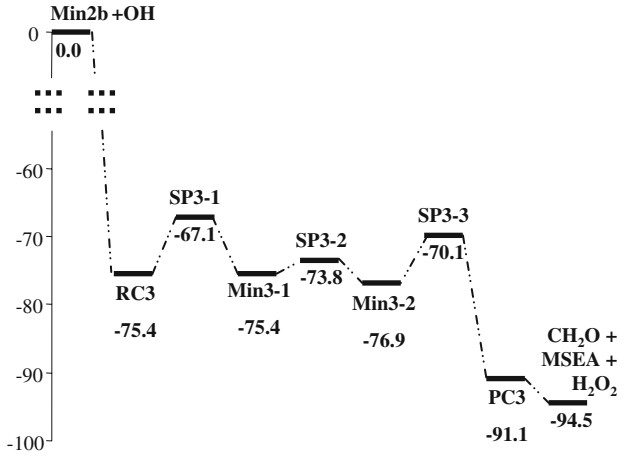

Fig. 3 CCSD(T)/MG3S/MPW1K/MG3S Gibbs free energy (kcal/mol) profile at 298 K for the reaction R3

group has lost its interaction with the sulfur atom (S···OOH distance of 2.264 Å), the hydroxylic hydrogen atom of the CH_2OH group is already almost bonded to OOH (H···OOH distance of 1.131 Å), while the CH_2O···H distance has clearly increased. Moreover, the S···CH_2O distance is also longer. At the PC3 structure, MSEA, CH_2O, and H_2O_2 are completely formed. Finally, the PC3 structure dissociates into these three products, with a free energy of reaction of −94.5 kcal/mol (see Fig. 3), so being the whole pathway thermodynamically feasible. In addition, the dynamical bottleneck of the whole process is located in the region corresponding to the formation of the initial RC3 complex as the rest of stationary points lie quite below reactants in terms of free energy (see Fig. 3). This means that, once Min2b is reached, this OH attack leading to MSEA formation would also be kinetically feasible.

As can be observed in Figures S4 and S5 included in the Supplementary Material, the reaction R4 is initiated from both, Min2a and Min2b, via two competitive channels that lead to the same reactant complex Min4-1 by means of the saddle points SP4-1a and SP4-1b, respectively. From Min2a/Min2b to Min4-1 the HOO fragment reorients and exchanges its OOH···CH_2 interaction by a new HOO···CH_2 one. This intramolecular reorganization takes place with a very high energy barrier (see Table S2 and Figure S5), but Min4-1 is thermodynamically accessible and clearly favored with respect to Min2a/Min2b. Note that the Min4-1 structure is similar to Min2a in terms of the orientation of the hydroxyl group, bonded to the sulfur atom, which is pointing to the opposite face of the two methyl groups. This fact is correlated with the S···OH distance. The tendency observed in this kind of structures which present the interaction S···OH is that the larger the S···OH bond distance, the less likely is that the OH and methyl groups are oriented to the same side of the molecule. From Min4-1, the reaction proceeds through a saddle point, SPMin4, that connects Min4-1 with a new conformer denoted Min4-2. The geometrical difference between those two minima is the value of the dihedral angle SOOH. Once Min4-2 is reached, MSEA formation is possible through the saddle point SP4-2, at 14.8 kcal/mol above DMS-OH + O_2 in terms of free energy, in which the S···CH_2OOH distance has started to increase. The MEP performed from SP4-2 leads to the PC4-1 structure in which MSEA and CH_2OOH are completely formed, although they still maintain a long-range interaction. At this point, the PC4-1 complex can either isomerise, yielding the PC4-2 (the same structure as PC1) minimum energy structure in which CH_3OO is formed from the CH_2OOH fragment, or can directly dissociate into the final products, MSEA and CH_2OOH. The isomerization takes place via the SP4-3 structure with a very high free energy barrier (29.1 kcal/mol with respect to DMS-OH + O_2) and once PC4-2 is formed, it directly dissociates into the final products, MSEA and CH_3OO. It is likely that tunneling effects along this intramolecular hydrogen-transfer path could accelerate somehow the isomerization rate. In contrast, the dissociation path from

PC4-1 takes place without classical or adiabatic potential energy barrier. According to the Gibbs free energy profile, the final products from the dissociation of both complexes, PC4-1 and PC4-2, are thermodynamically available, although the CH_3OO radical is favored versus its isomer CH_2OOH by 13 kcal/mol in terms of free energy. Nevertheless, due to the high free-energy barriers encountered along the reaction pathway, R4 does not seem to be a kinetically competitive process for MSEA formation.

The last pathway considered here is the reaction denoted as R5. The previous processes analyzed in this work lead to the formation of MSEA. This channel, in contrast, yields to DMSO formation. In one of our previous papers [26], the most feasible DMSO formation pathways were already studied. Nevertheless, the region of the potential energy surface explored in this work was not analyzed previously as the R5 reaction initiates from a conformer of $CH_3S(OH)CH_2(HO_2)$ (Min2a). This pathway has been included in the present work because it could compete with the MSEA formation channels R3 and R4. The R5 pathway leads from Min2a to a product complex PC5 via a unique saddle point denoted as SP5. The geometries of SP5 and PC5 are included in the Supplementary Material, but the classical and adiabatic potential energies for the whole process are given in Table 4. The R5 reaction pathway mainly consists in the intramolecular H-transfer from the OH group bonded to the sulfur atom in Min2b to the methylenic CH_2 group along with the disappearance of the HOO···CH_2 interaction. At the SP5 structure, the H-transfer is still taking place, but it is completed at PC5 which is an intermolecular complex between OOH and DMSO, the two final bimolecular products of the R5 pathway. The values in Table 4 and the free energy barrier depicted in Fig. 4 clearly indicate that this DMSO formation pathway could not be kinetically competitive even though the lifetime of Min2a was long enough and tunneling effects were taken into account for this intramolecular H-transfer process. Finally, it has to be pointed out that the energy values at the M05-2X/MG3S level compare better in general with the CCSD(T)/MG3S//MPW1K/MG3S values for reactions R2, R3, R4, and R5 than the corresponding MPW1K/MG3S results (see Tables 2, 3, 4 and S2).

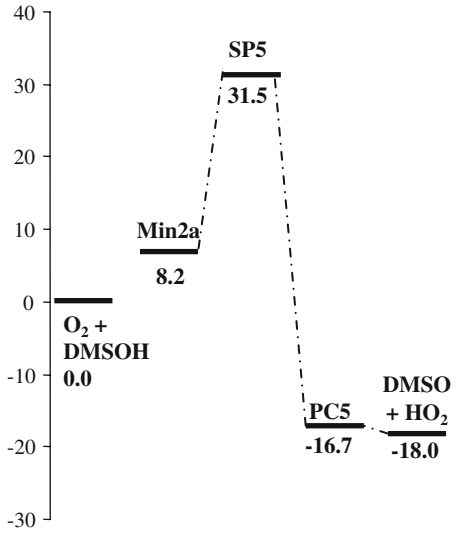

Fig. 4 CCSD(T)/MG3S/MPW1K/MG3S Gibbs free energy (kcal/mol) profile at 298 K for the reaction R5

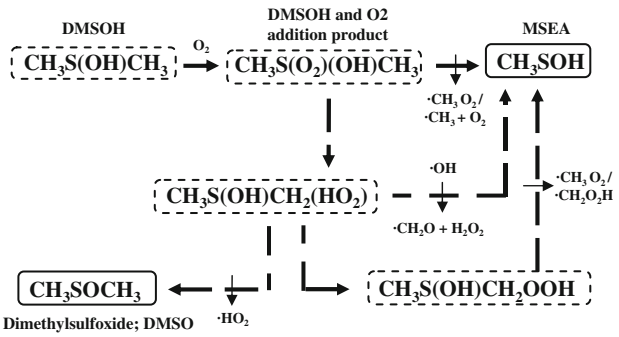

Fig. 5 Simplified reaction scheme of the studied pathways for MSEA and DMSO formation

In summary, it can be concluded that our theoretical results clearly show the existence of several reaction pathways leading to the formation of MSEA, all of them implying the prior formation of the $CH_3S(O_2)(OH)CH_3$ adduct formed by the addition of O_2 to the $CH_3S(OH)CH_3$ adduct, first intermediate of the OH-initiated addition channel of DMS oxidation. In Fig. 5, the reaction pathways studied in this work are summarized. The high energy barriers encountered along the R1 pathway, that represents

Table 4 Energies of the stationary points for the reaction R5 at different levels of calculation

	V_{Min2a}	$(V_a^G)_{Min2a}$	$V_{SP5}^{\ddagger}$	$(V_a^G)_{SP5}^{\ddagger}$	V_{PC5}	$(V_a^G)_{PC5}$	$V_{DMSO+HO_2}$	$(V_a^G)_{DMSO+HO_2}$
MPW1K/MG3S	0.9	3.0	28.8	27.9	−25.0	−22.1	−19.2	−17.8
M05-2X/MG3S	−2.4	−0.1	26.2	25.1	−24.7	−22.5	−18.2	−17.1
CCSD(T)/MG3S//MPW1K/MG3S	−1.8	0.3	25.0	24.1	−27.3	−24.4	−20.2	−18.7

V and V_a^G stand for the classical potential energies and the adiabatic potential energies, respectively. All energies (in kcal/mol) are relative to DMS-OH + O2

the dissociation of the $CH_3S(O_2)(OH)CH_3$ adduct by carbon sulphur bond cleavage, indicates that it is not a kinetically feasible pathway, in disagreement with previous suggestions by other authors indicating that the presence of the O_2 group in this adduct should facilitate C···S bond cleavage. Our results indicate that the most kinetically feasible process for MSEA formation would need of a previous intramolecular H-transfer in the $CH_3S(O_2)(OH)CH_3$ adduct (R2 reaction) leading to the $CH_3S(OH)CH_2(HO_2)$ complex. This latter adduct would then proceed (R3 reaction) with a high rate constant via its reaction with the OH radical, leading finally to three dissociated products: MSEA, CH_2O, and H_2O_2, in a thermodynamically favorable process. The viability of the R3 reaction pathway depends, however, on the rate constant of the previous R2 reaction, with a free energy barrier of around 10 kcal/mol with respect to DMS-OH + O_2, and to the population of the Min2b conformer of the $CH_3S(OH)CH_2(HO_2)$ complex, whose formation turns out to be endoergonic with respect to the $CH_3S(O_2)(OH)CH_3$ adduct.

Acknowledgments We are grateful for financial support from the Spanish "Ministerio de Ciencia y Tecnología", and the "Fondo Europeo de Desarrollo Regional" through project No. CTQ2005-07115/BQU, from the "Generalitat de Catalunya" (2005SGR00400), and the use of the computational facilities of the CESCA.

References

1. Atkinson R, Perry RA, Pitts J (1978) Chem Phys Lett 54:14. doi:10.1016/0009-2614(78)85653-X
2. Wine PH, Kreutter NM, Gump CA, Ravishankara AR (1981) J Phys Chem 85:266. doi:10.1021/j150618a019
3. Barone SB, Turnipseed AA, Ravishankara AR (1996) J Phys Chem 100:14694. doi:10.1021/jp960866k
4. Turnipseed AA, Barone SB, Ravishankara AR (1996) J Phys Chem 100:14703. doi:10.1021/jp960867c
5. Librando V, Tringalia G, Hjorth J, Coluccia S (2004) Environ Pollut 127:403. doi:10.1016/j.envpol.2003.08.003
6. Butkovskaya NI, LeBras G (1994) J Phys Chem 98:2582. doi:10.1021/j100061a014
7. Barnes I, Hjorth J, Mihalopoulos N (2006) Chem Rev 106:940. doi:10.1021/cr020529+
8. Uchimaru T, Tsuzuki S, Sugie M, Tokuhashi K, Sekiya A (2006) Chem Phys 324:465. doi:10.1016/j.chemphys.2005.11.018
9. Charlson RJ, Lovelock JE, Andreae MO, Warren SG (1987) Nature 326:655. doi:10.1038/326655a0
10. Andreae MO (1990) Mar Chem 30:1. doi:10.1016/0304-4203(90)90059-L
11. Yin F, Grosjean D, Seinfeld JH (1990) J Atmos Chem 11:309. doi:10.1007/BF00053780
12. Tyndall G, Ravishankara AR (1991) Int J Chem Kinet 23:483. doi:10.1002/kin.550230604
13. Barnes I, Bastian V, Becker KH (1988) Int J Chem Kinet 20:415. doi:10.1002/kin.550200602
14. Williams MB, Campuzano-Jost P, Cossairt BM, Hynes AJ (2007) J Phys Chem A 111:89. doi:10.1021/jp063873+
15. Silvente E, Richter RC, Hynes AJ (1997) J Chem Soc Faraday Trans 93:2821. doi:10.1039/a702575k
16. Williams MP, Campuzano-Jost P, Bauer D, Hynes A (2001) J Chem Phys Lett 344:61. doi:10.1016/S0009-2614(01)00764-3
17. Albu M, Barnes I, Becker KH, Patroescu-Klotz I, Mocanu R, Bentera T (2006) Phys Chem Chem Phys 8:728. doi:10.1039/b512536g
18. Hynes AJ, Wine PH, Semmes DH (1986) J Phys Chem 90:4148. doi:10.1021/j100408a062
19. Hynes AJ, Stocker RB, Pounds AJ, Mckay T, Bradshaw JD, Nicovich JM, Wine PH (1995) J Phys Chem 99:16967. doi:10.1021/j100046a024
20. McKee ML (1993) J Phys Chem 97:10971. doi:10.1021/j100144a013
21. Wang L, Zhang J (2001) J Mol Struct 543:167 TEOCHEM
22. Gross A, Barnes I, Sorensen RM, Kongsted J, Mikkelsen KV (2004) J Phys Chem A 108:8659. doi:10.1021/jp048852z
23. González-García N, González-Lafont À, Lluch JM (2005) J Comput Chem 26:569. doi:10.1002/jcc.20190
24. González-García N, González-Lafont À, Lluch JM (2006) J Phys Chem A 110:798. doi:10.1021/jp054424x
25. González-García N, González-Lafont À, Lluch JM (2007) ChemPhysChem 8:255. doi:10.1002/cphc.200600398
26. Ramírez-Anguita JM, González-Lafont À, Lluch JM (2009) J Comput Chem 30:173. doi:10.1002/jcc.21049
27. Sorensen S, Falbe-Hansen H, Hjorth J (1996) J Atmos Chem 24:299. doi:10.1007/BF00210288
28. Patroescu IV, Barnes I, Becker KH, Mihalopoulos N (1999) Atmos Environ 33:25. doi:10.1016/S1352-2310(98)00120-4
29. Arsene C, Barnes I, Becker KH, Mocanu R (2001) Atmos Environ 35:3769. doi:10.1016/S1352-2310(01)00168-6
30. Gross A, Baklanov A (2004) Int J Environ Pollut 22:51
31. Gunnarsson O, Lundqvist BI (1976) Phys Rev B 13:4274. doi:10.1103/PhysRevB.13.4274
32. Kohn W, Becke AD, Parr RG (1996) J Phys Chem 100:12974. doi:10.1021/jp960669l
33. Becke AD (1993) J Chem Phys 98:5648. doi:10.1063/1.464913
34. Langreth DC, Perdew JP (1977) Phys Rev B 15:2884. doi:10.1103/PhysRevB.15.2884
35. Zhao Y, Truhlar DG (2004) J Phys Chem A 108:6908. doi:10.1021/jp048147q
36. Zhao Y, Truhlar DG (2005) J Phys Chem A 109:5656. doi:10.1021/jp050536c
37. Zhao Y, Schultz NE, Truhlar DG (2005) J Chem Phys 123:161103. doi:10.1063/1.2126975
38. Zhao Y, Schultz NE, Truhlar DG (2006) J Chem Theory Comput 2:364. doi:10.1021/ct0502763
39. Frisch M, Pople JA, Binkley JS (1984) J Chem Phys 80:3265. doi:10.1063/1.447079
40. Lynch BJ, Zhao Y, Truhlar DG (2003) J Phys Chem A 107:1384. doi:10.1021/jp021590l
41. Esseffar M, Mó O, Yáñez M (1994) J Chem Phys 101:2175. doi:10.1063/1.467723
42. Timoshkin A, Frenking G (2000) J Chem Phys 113:8430. doi:10.1063/1.1318749
43. Resende SM, Ornellas FR (2002) J Braz Chem Soc 13:565. doi:10.1590/S0103-50532002000500004
44. Fast PL, Truhlar DG (2000) J Phys Chem A 104:6111. doi:10.1021/jp000408i
45. Truhlar DG, Kupperman A (1971) J Am Chem Soc 93:1840. doi:10.1021/ja00737a002
46. Fukui K (1982) Pure Appl Chem 54:1825. doi:10.1351/pac198254101825
47. Raghavachari K, Trucks GW, Pople JA, Heard-Gordon M (1989) Chem Phys Lett 157:479. doi:10.1016/S0009-2614(89)87395-6

48. Raghavachari K, Anderson JB (1996) J Phys Chem 100:12960. doi:10.1021/jp953749i
49. Zheng J, Gour JR, Lutz JJ, Włoch M, Piecuch P, Truhlar DG (2008) J Chem Phys 128:44108. doi:10.1063/1.2825596
50. Zhao Y, Lynch BJ, Truhlar DG (2004) J Phys Chem A 108:2715. doi:10.1021/jp049908s
51. Zhao Y, Truhlar DG (2008) Theor Chem Acc 120:215. doi:10.1007/s00214-007-0310-x
52. Frisch MJ, Trucks GW, Schlegel HB, Scuseria GE, Robb MA, Cheeseman JR, Montgomery JAJ, Vreven T, Kudin KN, Burant JC, Millam JM, Iyengar SS, Tomasi J, Barone V, Mennucci B, Cossi M, Scalmani G, Rega N, Petersson GA, Nakatsuji H, Hada M, Ehara M, Toyota K, Fukuda R, Hasegawa J, Ishida M, Nakajima T, Honda Y, Kitao O, Nakai H, Klene M, Li X, Knox JE, Hratchian HP, Cross JB, Bakken V, Adamo C, Jaramillo J, Gomperts R, Stratmann RE, Yazyev O, Austin AJ, Cammi R, Pomelli C, Ochterski JW, Ayala PY, Morokuma K, Voth GA, Salvador P, Dannenberg JJ, Zakrzewski VG, Dapprich S, Daniels AD, Strain MC, Farkas O, Malick DK, Rabuck AD, Raghavachari K, Foresman JB, Ortiz JV, Cui Q G. BA, Clifford S, Cioslowski J, Stefanov BB, Liu G, Liashenko A, Piskorz P, Komaromi I, Martin RL, Fox DJ, Keith T, Al-Laham MA, Peng CY, Nanayakkara A, Challacombe M, Gill PMW, Johnson B, Chen W, Wong MW, Gonzalez C, Pople JA (ed) (2003) In: GAUSSIAN03 RBG, Inc., Pittsburgh, PA
53. González C, Schlegel HB (1989) J Chem Phys 90:2154. doi:10.1063/1.456010
54. Corchado JC, Chuang Y-Y, Coitiño EL, Ellingson BA, Zheng J, Truhlar DG (2007) GAUSSRATE 9.7. University of Minnesota, Minneapolis
55. Page M, McIver JW (1988) J Chem Phys 88:922. doi:10.1063/1.454172
56. Melissas VS, Truhlar DG, Garrett BC (1992) J Chem Phys 96:5758. doi:10.1063/1.462674